JOURNAL OF GEOPHYSICAL RESEARCH, VOL. 99, NO. C5, PAGES 9767–9784, MAY 15, 1994

Hydrodynamic modulation of short wind-wave spectra by long waves and its measurement using microwave backscatter

Tetsu Hara
Graduate School of Oceanography, University of Rhode Island, Narragansett

William J. Plant
Applied Physics Laboratory, University of Washington, Seattle

Abstract. In this paper we use results of microwave backscattering experiments over the past decade to attempt to present a coherent picture of the ocean wave-radar modulation transfer function (MTF) based on composite surface theory, short-wave modulation, and modulated wind stress. A simplified relaxation model is proposed for the modulation of the gravity-capillary wavenumber spectrum by long waves. The model is based on the relaxation rate and the equilibrium gravity-capillary wavenumber spectrum. It differs from previous models by including all airflow modulation effects in the response of the equilibrium spectrum to changes in the airflow. Thus the explicit modulation of individual source functions such as wind input, short-wave dissipation, and nonlinear interactions need not be known in order to calculate the hydrodynamic MTF. By combining this new model of the hydrodynamic MTF with microwave measurements, we attempt to determine wind shear stress modulation caused by the long waves. In order to extract the hydrodynamic MTF from the microwave data, we remove tilt and range change effects from the measured MTFs using the published analytical forms for these effects. Our results show that the inferred hydrodynamic MTF is higher for H polarization scattering than for V polarization. Since this is impossible if we have obtained the true hydrodynamic MTF, these results strongly indicate a problem with composite scattering theory as it has been traditionally applied. One explanation for this result may be the effects of intermediate-scale waves suggested by Romeiser et al. (1993). Since these effects are much stronger for H polarization than for V polarization, they may explain our observed discrepancy and, if so, imply that V polarization return should yield an acceptable upper limit for the true hydrodynamic MTF. Thus we incorporate our V polarization results into the proposed model to estimate an upper limit for the wind shear stress modulation along the long-wave profile. We infer that the primary source of modulation of Bragg resonant waves depends strongly on Bragg wavenumber and windspeed. For low values of these quantities, straining by long-wave orbital velocities dominates the modulation process, while for higher values modulated wind stress becomes increasingly important. Our calculations indicate that wind stress modulation dominates the process for 3 cm Bragg waves at moderate to high wind speeds.

1. Introduction

Active microwave systems are powerful tools with which to observe dominant ocean surface waves since the instruments can be mounted remotely in various locations such as sea-based platforms, ships, aircraft, or satellites. One method of detecting dominant waves is through the modulation transfer function (MTF), originally introduced by *Keller and Wright* [1975] and defined as a linear frequency response function where input is the long-wave orbital velocity normalized by the long-wave phase velocity and the output is the AM part of the radar return normalized by its mean.

Several field measurements of the MTF have been performed mainly from research platforms [e.g., *Wright et al.*, 1980; *Plant et al.*, 1983; *Keller et al.*, 1985; *Schröter et al.*, 1986; *Keller and Plant*, 1990] where the long-wave orbital velocity is determined from the FM part of the radar return and is correlated with the AM part, yielding an estimate of the MTF. Al-

Paper number 93JC03514.
0148-0227/94/93JC-03514$05.00

though qualitative features of the MTF are consistent in all measurements and fairly well understood, quantitative agreement between different experiments has not been well confirmed, mainly because the MTF depends on so many parameters (e.g., microwave length, radar polarization, incidence angle, wind angle, wind speed, long-wave angle, long-wave frequency, long-wave mean square height/slope, air-sea temperature difference, etc.) and every experiment covers a slightly different regime.

According to composite surface theory the MTF consists of three components, that is, hydrodynamic MTF, tilt MTF, and range-change MTF [*Plant*, 1989] where the hydrodynamic MTF is the modulation of the wavenumber spectrum at the Bragg resonant wavenumber, and the latter two components are purely geometric effects due to the motion of the illuminated surface relative to the radar. If the shape of the wavenumber spectrum around the Bragg wavenumber is given, it is straightforward to subtract the two geometric effects. The resulting hydrodynamic MTF is evidently a better quantity to use for comparison between different experiments since it only depends on the Bragg wavenumber and environmental conditions and not on the configuration of the microwave system.

The hydrodynamic MTF is of scientific interest since it directly indicates how the short wind wave spectrum is modulated by long waves. This modulation not only affects a wide variety of active microwave systems [*Plant*, 1989] but is also crucial to understanding momentum transfer across the air-sea interface and thus to the development of waves and currents. The hydrodynamic MTF was first derived theoretically by *Keller and Wright* [1975] on the basis of the transport equation for the energy spectrum. They were followed by *Alpers and Hasselmann* [1978], who used the wave action conservation equation. Later *Wright et al.* [1980] indicated the importance of the shear stress modulation along the long-wave profile when the short-wave growth rate is large relative to the long-wave frequency. *Smith* [1990] also postulated the importance of shear stress modulation but also included the modulation of gravity and the shear current in his work. Quantitative comparison between these theoretical predictions and experimental results is not straightforward, however, because the models contain so many unknown parameters, in particular the nonlinear wave-wave interaction and the nonlinear dissipation rate of short wind waves and their modulations due to long waves are virtually unknown.

In this paper we first rederive the form for the hydrodynamic MTF based on composite surface theory (section 2.1) and present a simplified relaxation model based on the idea of an equilibrium wavenumber spectrum (section 2.2). According to this model the hydrodynamic MTF can be estimated without detailed knowledge of nonlinear wave interaction or wave dissipation as long as the relaxation rate and the equilibrium wavenumber spectrum are known. In section 3 we calculate the hydrodynamic MTF using X band microwave return from both the Marine Remote Sensing Experiment (MARSEN) and Synthetic Aperture Radar and X Band Ocean Nonlinearities (SAXON) - Forschungsplatform Nordsee (FPN) experiments and examine whether the results are consistent between vertical (V pol) and horizontal (H pol) radar polarizations, among different radar incidence angles, and between the two experiments carried out more than a decade apart. We will show that the hydrodynamic MTF derived from H pol return is significantly larger than that of V pol. Possible reasons for the observed deviation are discussed. Next in section 4 the modulation of wind shear stress along the long-wave profile is estimated on the basis of the proposed relaxation model and the observed hydrodynamic MTF of X band V pol return for both normally and obliquely incident waves and wind. Finally, in section 5 the hydrodynamic MTF from the Gulf of Mexico experiment is shown to be significantly larger than those from MARSEN or SAXON-FPN under neutral to stable atmospheric stratification. We suspect that the presence of surface contamination is the source of the difference.

2. Definition and Derivation of the MTF

2.1. Definition of the MTF and Geometric Effects

In this section we first summarize some of the definitions related to the modulation transfer function (MTF), following *Plant* [1989]. The underlying assumption is that both the long waves and the resulting modulation of the radar return are small perturbations and that they are linearly correlated. Past field observations indicate that this is a good approximation in many natural ocean conditions, and the concept of the MTF has proved to be very useful in various radar remote sensing techniques. Of course the linear assumption eventually breaks down as the nonlinearity of the long waves increases, in particular with the presence of wave breaking. Therefore caution is required when the concept is applied to a high-sea state. In the following derivations we use the linear long-wave theory and all the second-order terms are neglected.

Let us define (x, y) as horizontal coordinates, z as a vertically upward coordinate measured from the mean water level, and ϕ as the angle measured from the positive x axis in the counterclockwise direction. We set the antenna look direction to be in the positive x direction ($\phi = 0$) and the center of the illuminated area at $x = y = 0$. The water depth, the antenna incident angle, and the antenna height are denoted by d, θ, and h, respectively. The wind direction (from which wind blows) is denoted by ϕ_{wd} and the wave direction (from which long waves propagate) by ϕ_{wv}, both angles being measured counterclockwise from the x axis.

The horizontal long-wave orbital velocity U at the ocean surface and the microwave radar return P are now written in terms of the Fourier series

$$U = \sum_{\Omega} \tilde{U}(\Omega) e^{i\Omega t} \tag{1}$$

and

$$P = \bar{P} + \sum_{\Omega} \tilde{P}(\Omega) e^{i\Omega t} \tag{2}$$

where Ω is the discrete angular frequency and the overbar denotes the time average. Then the MTF m and the coherence γ^2 are defined as

$$m(\Omega) = \frac{C(\Omega)}{\bar{P}} \frac{G_{PU}(\Omega)}{G_{UU}(\Omega)} \tag{3}$$

and

$$\gamma^2(\Omega) = \frac{|G_{PU}(\Omega)|^2}{G_{UU}(\Omega) G_{PP}(\Omega)} \tag{4}$$

where C is the long-wave phase velocity based on the linear theory. The one-sided cross-spectral (autospectral) density is defined as

$$G_{PU} = 2T < \tilde{P}\tilde{U}^* > \tag{5}$$

where T is the time record length, angle brackets are the ensemble average, and asterisks denote the complex conjugate.

The derivation of the MTF based on composite surface theory has been reported in many places including *Plant* [1989]. We start from the assumption that the microwave return in the intermediate incidence angle range is mostly due to Bragg scattering, an assumption we believe to be amply justified at low to moderate winds by past studies [*Keller and Plant*, 1990]. Let us define the folded two-dimensional short-wave wavenumber spectrum as

$$\psi(k, \phi) \equiv F(k, \phi) + F(k, \phi + \pi) \tag{6}$$

where k is the wavenumber and F is the conventional wavenumber spectrum. Then the beam-limited radar return power without the long-wave modulation is

$$P \propto \frac{\sigma_o A}{R_i^4} \tag{7}$$

where the normalized cross section σ_o is

$$\sigma_o = 16\pi k_o^4 \Gamma(\theta) \psi(k = 2k_o \sin\theta, \phi = 0) \tag{8}$$

and the illuminated area is

$$A = \frac{R_i^2 \Phi_V \Phi_H}{2 \cos\theta} \tag{9}$$

The range between the antenna and the sea surface is denoted by R_i, the microwave wavenumber by k_o, and one-way, half-power, full-width antenna beamwidths in the vertical and horizontal by Φ_V and Φ_H, respectively. The Bragg scattering geometric coefficient Γ is approximately

$$\Gamma(\theta) \doteq \frac{\cos^4\theta (1 + \sin^2\theta)^2}{(\cos\theta + 0.111)^4} \tag{10}$$

for vertical polarization and

$$\Gamma(\theta) \doteq \frac{\cos^4\theta}{(0.111 \cos\theta + 1)^4} \tag{11}$$

for horizontal polarization for a dielectric constant of 81, which is appropriate for the sea surface over a wide range of microwave frequencies [*Plant*, 1989, 1990].

To the leading order the modulation of the return power due to long waves, denoted by δP, is then

$$\frac{\delta P}{\bar{P}} = \frac{\delta\psi}{\bar{\psi}} + \left(\frac{1}{\Gamma} \frac{d\Gamma}{d\theta} + \tan\theta + \frac{1}{\tan\theta} \frac{k}{\bar{\psi}} \frac{\partial \bar{\psi}}{\partial k} \right) \delta\theta - \frac{2}{R_i} \delta R_i + \left(\frac{1}{\bar{\psi}} \frac{\partial \bar{\psi}}{\partial \phi} \right) \delta\phi \tag{12}$$

where $\delta\psi$ is the hydrodynamic modulation of the folded wavenumber spectrum at the fixed resonant wavenumber, that is, at $k = 2k_o \sin\theta$ and $\phi = 0$. Here we have used the fact that the quantity without the long-wave modulation is equal to the time-averaged quantity to the leading order. The time average of the folded spectrum $\bar{\psi}$ and its derivatives are also evaluated at $k = 2k_o \sin\theta$ and $\phi = 0$. The perturbation δR_i, $\delta\theta$, $\delta\phi$ are further related to the long-wave height ζ and its derivatives by

$$\frac{\delta R_i}{R_i} = -\frac{\zeta}{h} \tag{13}$$

$$\delta\theta = -\frac{\partial \zeta}{\partial x} \tag{14}$$

$$\delta\phi = -\frac{1}{\tan\theta} \frac{\partial \zeta}{\partial y} \tag{15}$$

again to the leading order.

Let us write the long-wave orbital velocity as

$$U = \sum_{\Omega} \tilde{U}(\Omega) e^{i(K \cos\phi_{wv} x + K \sin\phi_{wv} y + \Omega t)} \tag{16}$$

which reduces to (1) at the center of the illuminated area $x = y = 0$. On the basis of the linear theory the wavenumber of the long waves K is related to Ω by

$$\Omega^2 = gK \tanh Kd \tag{17}$$

and the long-wave height ζ and its derivatives at $x = y = 0$ are given as

$$\zeta = \sum_{\Omega} \frac{\tilde{U}}{C} \frac{\tanh Kd}{K} e^{i\Omega t} \tag{18}$$

$$\frac{\partial \zeta}{\partial x} = \sum_{\Omega} \frac{\tilde{U}}{C} i \cos\phi_{wv} \tanh Kd\, e^{i\Omega t} \tag{19}$$

$$\frac{\partial \zeta}{\partial y} = \sum_{\Omega} \frac{\tilde{U}}{C} i \sin\phi_{wv} \tanh Kd\, e^{i\Omega t} \tag{20}$$

Substituting (12)–(15) and (18)–(20) into (3), we obtain the total MTF which consists of three parts:

$$m = m' + m_r - i\, m_t \tag{21}$$

where

$$m' = \frac{C}{\bar{\psi}} \frac{G_{\psi U}}{G_{UU}} \tag{22}$$

$$m_r = 2 \frac{\tanh Kd}{Kh} \tag{23}$$

$$m_t = \left(\frac{1}{\Gamma}\frac{d\Gamma}{d\theta} + \tan\theta + \frac{1}{\tan\theta}\frac{k}{\bar{\psi}}\frac{\partial\bar{\psi}}{\partial k}\right) \times \tanh Kd\cos\phi_{wv} + \left(\frac{1}{\tan\theta}\frac{1}{\bar{\psi}}\frac{\partial\bar{\psi}}{\partial\phi}\right)\tanh Kd\sin\phi_{wv} \quad (24)$$

Complex notation is used to conveniently keep track of phase: The positive real part is in phase with the long-wave height and the positive imaginary part is 90° ahead of the long-wave height. The first term m' in (21) is the hydrodynamic MTF and corresponds to the modulation of the folded wavenumber spectrum of Bragg resonant waves. Therefore this quantity depends only on the resonant Bragg wavenumber and other environmental conditions. The second term m_r (height MTF) is due to the modulation of the range between illuminated area and the radar. This term is real and negligibly small in most cases. The last term im_t (tilt MTF) appears because the effective resonant wavenumber is modified by the slope of long waves. This quantity is purely imaginary and depends on the radar polarization and on incidence angle, as well as on the derivatives of the folded wavenumber spectrum. Both m_r and m_t are purely geometric effects.

In order to calculate the tilt MTF, it is necessary to introduce the functional form of the folded wavenumber spectrum $\bar{\psi}$. Comprehensive measurements of the wavenumber spectrum of short wind waves in a wave tank have recently been performed by *Jähne and Riemer* [1990]. Their results show that the slope of the wavenumber spectrum is roughly between $k^{-3.5}$ and k^{-5} in all directions for wind speed between $2.7\,\mathrm{m\,s^{-1}}$ and $17.2\,\mathrm{m\,s^{-1}}$, and for $k \sim 3\,\mathrm{cm^{-1}}$ (X band). On the other hand, the directional spreading varies significantly for different wind speeds and wavenumbers. We therefore assume the following form of the folded spectrum $\bar{\psi}$:

$$\bar{\psi} \propto k^{-n}[\alpha + (1-\alpha)\cos^2(\phi - \phi_{wd})] \quad (25)$$

where $-n$ is the power of the slope of the spectrum and α is the measure of the directional spreading. These two parameters are allowed to vary within the following ranges:

$$3.5 \le n \le 5, \qquad 0.1 \le \alpha \le 1 \quad (26)$$

in the subsequent analyses. Introducing (10), (11), and (25) into (24), the tilt modulation is calculated to be

$$m_t = \left(-3\tan\theta + \frac{4\sin\theta\cos\theta}{1+\sin^2\theta} + \frac{4\sin\theta}{\cos\theta + 0.111} - \frac{n}{\tan\theta}\right)\tanh Kd\cos\phi_{wv} + \left(\frac{1}{\tan\theta}\frac{2(1-\alpha)\cos\phi_{wd}\sin\phi_{wd}}{\alpha + (1-\alpha)\cos^2\phi_{wd}}\right) \times \tanh Kd\sin\phi_{wv} \quad (27)$$

for vertical polarization, and

$$m_t = \left(-3\tan\theta + \frac{0.444\sin\theta}{0.111\cos\theta + 1} - \frac{n}{\tan\theta}\right) \times \tanh Kd\cos\phi_{wv} + \left(\frac{1}{\tan\theta}\frac{2(1-\alpha)\cos\phi_{wd}\sin\phi_{wd}}{\alpha + (1-\alpha)\cos^2\phi_{wd}}\right) \times \tanh Kd\sin\phi_{wv} \quad (28)$$

for horizontal polarization. We note that the tilt modulation becomes independent of the long-wave frequency in deep water ($Kd \to \infty$). The dependence of m_t on the incidence angle has been examined in *Alpers et al.* [1981] and *Plant* [1989] and is not repeated here. In general, the first term (due to tilt in the antenna look direction) is dominant over the second term (due to tilt perpendicular to the antenna look direction), and the value of m_t is negative in the range of n considered. Only when both the wind angle and the wave angle are close to ±90° and the spreading factor α is small does the second term become significant.

2.2 A Relaxation Model of the Hydrodynamic MTF

Once the geometric effects are subtracted from the total MTF, the remaining hydrodynamic MTF corresponds to the modulation of the wavenumber spectrum due to long waves. Past derivations of the hydrodynamic MTF by *Wright et al.* [1980] and *Smith* [1990], both of which include the effect of the modulated wind stress, were based on the wave action conservation equation with three forcing terms, namely, wind input, dissipation, and nonlinear interaction. In this approach the proper evaluation of the hydrodynamic MTF in principle requires the knowledge of all forcing terms and their modulation due to long waves, some of which are not available either theoretically or experimentally at present. Here we present a slightly simpler derivation of the hydrodynamic MTF and compare it with the former theories.

We start from the hypothesis that without long waves the equilibrium wavenumber spectrum is determined only by the wind shear stress [*Phillips*, 1985]. If for some reason the spectrum is disturbed, it returns to the equilibrium state with a certain relaxation rate. When long waves exist whose wavelength is much larger than the scale of the Bragg resonant waves, it is reasonable to assume that the wavenumber spectrum tends to approach the local equilibrium, which is determined by the local wind shear stress along the long-wave profile. The generalized action conservation equation is then written as

$$\frac{dN(\vec{k})}{dt} = \frac{\partial N}{\partial t} + \frac{\partial N}{\partial \vec{x}}\cdot\frac{\partial\sigma}{\partial\vec{k}} - \frac{\partial N}{\partial\vec{k}}\cdot\frac{\partial\sigma}{\partial\vec{x}} = \frac{\omega}{k}\int\int\beta(\vec{k}';\vec{k})[-F(\vec{k}') + F_{eq}(\vec{k}')]d\vec{k}' \quad (29)$$

where $k = |\vec{k}|$ is the wavenumber of the short waves, ω is the intrinsic angular frequency, $\sigma = \omega + \vec{k}\cdot\vec{U}$ is the

apparent angular frequency, $N = (\omega/k)F$ is the wave action density, and $\beta(\vec{k}';\vec{k})$ is the relaxation rate of the spectrum $F(\vec{k})$ due to the deviation of $F(\vec{k}')$ from its equilibrium $F_{eq}(\vec{k}')$. The second term $\frac{\partial N}{\partial \vec{x}} \cdot \frac{\partial \sigma}{\partial \vec{k}}$ is much smaller than the first term and is neglected in the following discussion. For short waves propagating close to the wind direction it is assumed that the effect of the deviation of the spectrum at a different wavenumber is negligible, that is,

$$\beta(\vec{k}';\vec{k}) \simeq \beta\delta(\vec{k}' - \vec{k}) \tag{30}$$

where δ is the Dirac delta function and the action conservation equation reduces to

$$\frac{dN(\vec{k})}{dt} = \frac{\omega}{k}\beta[-F(\vec{k}) + F_{eq}(\vec{k})] \tag{31}$$

This assumption may not hold for waves propagating perpendicular to the wind, since the nonlinear energy transfer rate from different wavenumbers may overwhelm the energy input rate from wind for those waves. The model also excludes the possible effect of intermediate-scale waves which are larger than Bragg waves but smaller than the modulating sources. Thus the model should not be applied, for example, for parasitic capillary waves which are strongly coupled with intermediate-scale waves.

Suppose the friction velocity u_* is modulated by long waves and is written as

$$u_* = \bar{u}_* + \sum_{\Omega} \tilde{u}_*(\Omega)e^{i\Omega t} \tag{32}$$

Then the actual wavenumber spectrum F and the local equilibrium wavenumber spectrum F_{eq} are also expanded in Fourier series:

$$F = \bar{F} + \sum_{\Omega} \tilde{F}(\Omega)e^{i\Omega t} \tag{33}$$

$$F_{eq} = \bar{F}_{eq} + \sum_{\Omega} \tilde{F}_{eq}(\Omega)e^{i\Omega t} = \bar{F} + \frac{\partial \bar{F}}{\partial \bar{u}_*} \sum_{\Omega} \tilde{u}_*(\Omega)e^{i\Omega t} \tag{34}$$

where $\bar{F} = \bar{F}_{eq} = F_{eq}(\bar{u}_*)$, and $\frac{\partial \bar{F}}{\partial \bar{u}_*} = \left.\frac{\partial F_{eq}}{\partial u_*}\right|_{\bar{u}_*}$ to first order. By introducing (16), (33), and (34) into (31), and evaluating it at $\phi = 0$ or π, it is straightforward to show that the ratio of the Fourier coefficient of the wavenumber spectrum divided by its mean is

$$\frac{\tilde{F}}{\bar{F}} = \left\{ -\frac{\tilde{U}}{C}\left[\left(\frac{k}{\bar{F}}\frac{\partial \bar{F}}{\partial k} + \frac{c_g}{c} - 1\right)\cos^2\phi_{wv} + \frac{1}{\bar{F}}\frac{\partial \bar{F}}{\partial \phi}\cos\phi_{wv}\sin\phi_{wv}\right] - i\frac{\beta}{\Omega}\frac{\tilde{F}_{eq}}{\bar{F}}\right\} \times \left(1 - i\frac{\beta}{\Omega}\right)^{-1} \tag{35}$$

to the leading order, where c and c_g are the phase and the group velocities of the short waves, respectively. Unless the wind direction is appreciably greater than zero, the spectrum of waves propagating against the wind is negligibly small:

$$F(k,\pi) \gg F(k,0) \tag{36}$$

that is,

$$\psi(k,0) \simeq F(k,\pi) \tag{37}$$

Therefore referring to the definition of the hydrodynamic MTF, (22), we obtain

$$m' \simeq \left\{ -\left[\left(\frac{k}{\bar{F}}\frac{\partial \bar{F}}{\partial k} + \frac{c_g}{c} - 1\right)\cos^2\phi_{wv} + \frac{1}{\bar{F}}\frac{\partial \bar{F}}{\partial \phi}\cos\phi_{wv}\sin\phi_{wv}\right] - i\frac{\beta}{\Omega}\left(\frac{C}{\bar{F}}\frac{G_{F_{eq}U}}{G_{UU}}\right)\right\} \times \left(1 - i\frac{\beta}{\Omega}\right)^{-1} \tag{38}$$

evaluated at $\phi = \pi$. For the wind angle near $\pm 90°$ this equation is also approximately valid if the derivatives of $\bar{F}$ are replaced by those of $\bar{\psi}$. This result for m' should be compared with the complex conjugate of those in earlier papers [*Keller and Wright*, 1975; *Wright et al.*, 1980]. The definition of m_t in (24) is also the complex conjugate of that given in the earlier papers; it agrees with the definition t in *Plant* [1989]. The present definitions of m' and m_t yield phase angles for m which are in agreement with experimental definitions; that is, positive phase implies that maximum modulation leads the crest of an approaching long wave. The square bracket in (38) is the effect of straining due to the long-wave orbital velocity. If the relaxation rate β is much larger than the long-wave angular frequency Ω, the hydrodynamic MTF m' is approximately

$$m' \sim m_\infty \equiv \frac{C}{\bar{F}}\frac{G_{F_{eq}U}}{G_{UU}} \tag{39}$$

which is the cross spectrum between the local equilibrium spectrum and the long-wave orbital velocity. We may rewrite m_∞ in terms of the cross spectrum between the friction velocity u_* and the long-wave orbital velocity U:

$$m_\infty = \frac{C}{\bar{F}}\frac{G_{F_{eq}U}}{G_{UU}} = \left(\frac{C}{\bar{u}_*}\frac{G_{u_*U}}{G_{UU}}\right)\left(\frac{\bar{u}_*}{\bar{F}}\frac{\partial \bar{F}}{\partial \bar{u}_*}\right) \tag{40}$$

where the second term is determined from the rate of change of the mean wavenumber spectrum versus the mean friction velocity.

In summary, the hydrodynamic MTF can be expressed in terms of the following four quantities: (1) the dependence of $\bar{F}$ (or $\bar{\psi}$) on k and ϕ, (2) the relaxation rate β, (3) the dependence of $\bar{F}$ on $\bar{u}_*$ (or the dependence of F_{eq} on u_*), and (4) the modulation of u_* along the long-wave profile. No explicit forms of forcing terms (wind input, nonlinear interaction, or dissipation) appear in these expressions. From past measurements, quantities 1 and 3 are fairly well understood. The relaxation rate β has been assumed to be either equal to

or twice as large as the linear growth rate in past literature, depending on the form of nonlinearity of the energy input/dissipation rate. However, conclusive values have not been obtained either experimentally or theoretically. Little is known about the last quantity, 4, for dominant ocean waves, although some laboratory data are available for shorter waves [*Hsu et al.*, 1981; *Hsu and Hsu*, 1983].

In order to compare our model with other theories, we rewrite the forcing term of (31) in terms of the sum of wind input, dissipation, and nonlinear transfer. Call this sum B. Then,

$$\frac{dN(\vec{k})}{dt} = \frac{\omega}{k}\mathrm{B}(F, u_*) \tag{41}$$

Since we are only considering linear infinitesimal perturbations from the mean, the time averaged quantities are equivalent to those in the equilibrium state, and they must satisfy

$$0 = \mathrm{B}(\bar{F}, \bar{u}_*) \tag{42}$$

Our relaxation rate β and the second term in (40) may then be written as

$$\beta = -\left.\frac{\partial \mathrm{B}}{\partial F}\right|_{\bar{F}} \tag{43}$$

$$\frac{\bar{u}_*}{\bar{F}}\frac{\partial \bar{F}}{\partial \bar{u}_*} = \left.\frac{\bar{u}_*}{\beta \bar{F}}\frac{\partial \mathrm{B}}{\partial u_*}\right|_{\bar{u}_*} \tag{44}$$

For example, if the total forcing consists of a linear growth rate β_1 and a nonlinear dissipation rate β_n of nth power, then B is written as

$$\mathrm{B} = \beta_1(u_*)F - \beta_n(u_*)F^n \tag{45}$$

with the equilibrium condition that

$$0 = \beta_1(\bar{u}_*)\bar{F} - \beta_n(\bar{u}_*)\bar{F}^n \tag{46}$$

Referring to (43) and (44) we obtain

$$\beta = (n-1)\beta_1(\bar{u}_*) \tag{47}$$

and

$$\frac{\bar{u}_*}{\bar{F}}\frac{\partial \bar{F}}{\partial \bar{u}_*} = \frac{\bar{u}_*}{(n-1)\beta_1}\left(\frac{\partial \beta_1}{\partial u_*} - \bar{F}^{n-1}\frac{\partial \beta_n}{\partial u_*}\right)_{u_*=\bar{u}_*} \tag{48}$$

Thus the relaxation rate β is equal to the linear growth rate β_1 multiplied by $n-1$, where n is the power of the nonlinear term in B.

Let us now compare our formulation (38) and (40) with past theories. Both *Keller and Wright* [1975] and *Alpers and Hasselmann* [1978] have assumed that the total forcing is proportional to the deviation of the spectrum from its mean; that is,

$$\mathrm{B} = \beta_1(F - \bar{F}) \tag{49}$$

with β_1 being negative and independent of u_*. Then the relaxation rate β is equal to $-\beta_1$ and the right-hand side of (48) is zero; the modulation of the spectrum disappears as β increases. Therefore these models are unrealistic for strong winds. The effect of modulated wind shear stress along the long-wave profile was first incorporated by *Wright et al.* [1980], who solved the coupled action conservation equations of Bragg resonant waves and much smaller capillary waves. After examining the order of magnitude of each term, their coupled equations were effectively reduced to the action conservation equation of the Bragg wavenumber only, with a linear growth rate β_1 and a quadratic dissipation rate β_2 which is independent of u_*,

$$\mathrm{B} = \beta_1(u_*)F - \beta_2 F^2 \tag{50}$$

Then (47) and (48) are reduced to

$$\beta = \beta_1(\bar{u}_*) \tag{51}$$

and

$$\frac{\bar{u}_*}{\bar{F}}\frac{\partial \bar{F}}{\partial \bar{u}_*} = \left.\frac{\bar{u}_*}{F_{eq}}\frac{\partial F_{eq}}{\partial u_*}\right|_{\bar{u}_*} = \left.\frac{\bar{u}_*}{\beta_1}\frac{\partial \beta_1}{\partial u_*}\right|_{\bar{u}_*} \tag{52}$$

to first order. Thus the relaxation rate is equal to the linear growth rate β_1 and the additional forcing term is directly related to the linear growth rate β_1 as a function of the friction velocity u_*. In general, the nonlinear term in B also depends on u_*. As a result, the linear growth rate β_1 and the equilibrium wavenumber spectrum F_{eq} may have different dependencies on u_* and (52) does not hold. Indeed *Jähne and Riemer* [1990] have shown that F_{eq} is proportional to $u_*^{2.5}$ for $k = 0.25$–$1\,\mathrm{cm}^{-1}$, and $u_*^{1.0}$ for $k = 2$–$8\,\mathrm{cm}^{-1}$, while the linear growth rate is known to be proportional to $u_*^{1.5}$ [*Larson and Wright*, 1975] or $u_*^{2.0}$ [*Plant*, 1982] in the same range of wavenumber.

Smith [1990] further incorporated the effect of the modulated drift and apparent gravity in order to model the total forcing B more accurately. If all the energy input/output terms are properly evaluated, his model will ultimately lead to the same result for the hydrodynamic MTF m' as our model. However, little is known about the nonlinear transfer rate or the dissipation rate of short wind waves at present. Therefore it is more practical to use the idea of equilibrium spectrum and the relaxation rate β, rather than modeling all the input/output terms and their modulations due to long waves.

3. Total and Hydrodynamic MTF From SAXON-FPN and MARSEN Data

3.1. Experimental Conditions

The MARSEN experiment took place in September and October of 1979 at the German Forschungsplatform Nordsee (FPN) in the North Sea. Both L band (at 12 m height) and X band (at 23/24 m height) microwave systems were mounted with varying incidence angles.

While some X band measurements were made with horizontal polarization (H pol), most of the measurements were performed with vertical polarization (V pol). Furthermore, the H pol measurements made during this experiment were not simultaneous with the V pol measurements. We will not consider MARSEN H pol data in this paper. Wind speed and direction were measured at 43 m above the mean water level. Wave fields were dominated by the locally generated wind waves, and the measured wind direction and visually determined wave direction were mostly within 30° of each other. The air-sea temperature difference was always within ±5°C. Other details of the experiment have been reported by *Plant et al.* [1983] and are not repeated here.

The SAXON-FPN experiment was performed in November, 1990 at the same research platform (FPN) as MARSEN. An overview of the SAXON-FPN experiment is given in *Plant and Alpers* [this issue]. Both X band and Ka band microwave systems were mounted at varying heights with the incidence angle near 45°. Measurements were made with both V pol and H pol simultaneously. In addition, a similar Ku band system was operated by Massachusetts Institute of Technology. It has been confirmed that the results of X band and Ku band are almost indistinguishable, and those of Ka band are very similar [*Keller and Plant*, 1990; *Plant et al.*, this issue (b)]. This is rather surprising since the resonant wavenumber for Ka band is roughly 9.5–12.6 cm^{-1} which is within the wavenumber range of parasitic capillaries, and the modulation mechanism can be quite different from the Bragg waves at X band. One possible explanation is that the parasitic wave generation is significant only within a limited range of wind stress (which is apparently true in wind-wave tanks). Thus in the field environment where wind stress is quite variable, the effect of parasitic wave generation may be overshadowed by direct generation by wind in most cases. Based on these preliminary analyses we present results only from the X band system in this study. The air-sea temperature difference varied between −8°C and +3°C and was mostly in the unstable to neutrally stable range. Wind speed and direction were measured at 47 m height. Directional long-wave spectra were measured by a Wavec pitch and roll buoy. In general, the long waves between 0.1 and 0.15 Hz were dominated by swell propagating from NW and were not affected by the local wind. On the other hand, the long waves beyond 0.25 Hz were mostly generated locally by wind, and their direction was always close to the wind direction. Between 0.15 and 0.25 Hz the direction of waves varied between the wind direction and the swell direction. In the following discussion we have defined the wave angle as the average angle of waves between 0.25 and 0.375 Hz, and have excluded data when the standard deviation of wave direction in this frequency range exceeds 30°.

The analysis procedure is identical for the data sets of both experiments. The long-wave orbital velocity (U) is calculated from the FM part of the radar return signal and the long-wave direction, which is determined visually (MARSEN) or from the buoy data (SAXON-FPN). The FFTs of the orbital velocity U and the return power P are calculated from a 64 s record at 64 discrete frequencies between 1/64 and 1 Hz. The product of the Fourier coefficients are then averaged for 20 consecutive records in order to estimate the autospectral/cross-spectral densities. Finally, the MTF and the coherence are calculated according to (3) and (4).

In the following figures the results are further averaged over the indicated ranges of different parameters. The 95% confidence levels of measured quantities are roughly estimated as

$$\hat{a}(1-2\epsilon) \le a \le \hat{a}(1+2\epsilon) \tag{53}$$

where $\hat{a}$ is the estimated value, a the true value, and ϵ the normalized random error [*Bendat and Piersol*, 1986]. The estimate of ϵ is given as

$$\epsilon(|\hat{m}|) = \epsilon[\Re(\hat{m})] = \epsilon[\Im(\hat{m})] = \left(\frac{1-\gamma^2}{2\gamma^2 n_d}\right)^{\frac{1}{2}} \tag{54}$$

for the amplitude or the real/imaginary part of the MTF(m),

$$\epsilon(\hat{\phi}_m) = \frac{\epsilon(|\hat{m}|)}{\phi_m} \tag{55}$$

for the phase of m, and

$$\epsilon(\hat{\gamma}^2) = \left[\frac{2(1-\gamma^2)}{\gamma^2 n_d}\right]^{\frac{1}{2}} \tag{56}$$

for the coherence γ^2, where n_d is the number of averaged records. Although these are no more than rough estimates of the confidence levels, they at least indicate the relative accuracies of the estimated values.

In most cases the coherence function turned out to be between 0.4 and 0.5 (sometimes between 0.3 and 0.6), which means roughly 40–50% of the modulation of the gravity-capillary wave spectrum at a given frequency is correlated with the corresponding long waves. These were also typical values in the past measurement of MTF in a field environment. Past analyses have suggested that the uncorrelated part of the modulation may be mostly associated with wind turbulence, that is, the low frequency component of air flow turbulence which is not correlated with the long waves but modulates the short gravity-capillary waves [*Plant et al.*, 1983]. In addition, the directional spreading and nonlinearity of the modulating long waves may reduce the coherence.

Past studies of the MARSEN MTFs have shown no dependence on the mean square long-wave slope/height [*Plant et al.*, 1983] and our present data do not seem to vary with this parameter either. Such dependence has been found in work in the Gulf of Mexico but only under stable atmospheric conditions [*Keller et al.*, 1985]. Since conditions in the North Sea in the fall, the times of both MARSEN and SAXON-FPN, are generally neutral to unstable, these two results seem to be consistent

with each other. We were also unable to detect a dependence of the SAXON-FPN MTFs on atmospheric stability over the range of stabilities which were obtained during the experiment . Therefore neither stability nor long-wave slope are restricted in Figures 1–12.

3.2. Comparison Between H pol and V pol

We first examine the results from SAXON-FPN. The real and imaginary parts of the total MTF m and the hydrodynamic MTF m' are shown in Figure 1 and Figure 2 for both V pol and H pol and for different wind speeds. Wind and wave directions are restricted to within $\pm 30^o$ of the antenna look direction (north). The results are averaged between 0.25 and 0.3125 Hz in long-wave frequency (f) and averaged for $\pm 0.5\,\mathrm{m\,s^{-1}}$ around the indicated wind speed (U_{wd}). Within each range of averaging the MTFs are found to be stationary in most cases. The hydrodynamic MTF m' has been calculated by subtracting the range change modulation (23) and the tilt modulation (27) or (28) from the measured total MTF m. Since we have allowed the parameters of the shape of the folded wavenumber spectrum to vary in (26), both the maximum and the minimum values of the tilt modulation m_t can be calculated. In Figures 2, 6–14 we show the hydrodynamic MTFs with both minimum m_t and maximum m_t, and the results from the maximum m_t are slightly shifted to the right. Note that only the imaginary part is affected by the tilt modulation.

We first notice that the "hydrodynamic" MTF m' is not the same when inferred from H pol measurements as it is when inferred from V pol measurements. Rather, the difference in the real parts is on the order of 4 while that of the imaginary parts is on the order of -4. The imaginary parts, however, are close to zero in both cases, which implies that the difference in the magnitudes of the hydrodynamic MTF at the two polarizations is nearly the same as that of the real parts. Since the range change MTF is small and tilt affects only the imaginary part of the MTF, this difference in the real parts is a direct result of the measurement, not of the subsequent removal of geometric effects. Since the hydrodynamic MTF corresponds to the cross spectrum of the wave orbital velocity and the wavenumber spectrum of the Bragg resonant waves, it should not depend on polarization if the underlying theoretical assumptions are correct. These results therefore suggest that the MTF of at least one of the polarizations cannot be explained by composite surface theory as conventionally applied to MTF calculations. This result contrasts with *Plant et al.* [1983] where they conclude from the MARSEN data that composite surface theory explains the observed differences between H and V pol MTFs rather well except for a slight phase mismatch. However, as we pointed out above, measurements at these different polarizations were not made simultaneously during MARSEN. Furthermore, the results of *Jähne and Riemer* [1990] were not available in 1983 so the shape of the short-wave equilibrium spectrum near the X band Bragg wave was poorly estimated by *Plant et al.* [1983]. Thus we feel that the present results are more accurate and that the same hydrodynamic MTF cannot be derived from simultaneous measurements of H and V pol MTFs using the conventional application of com-

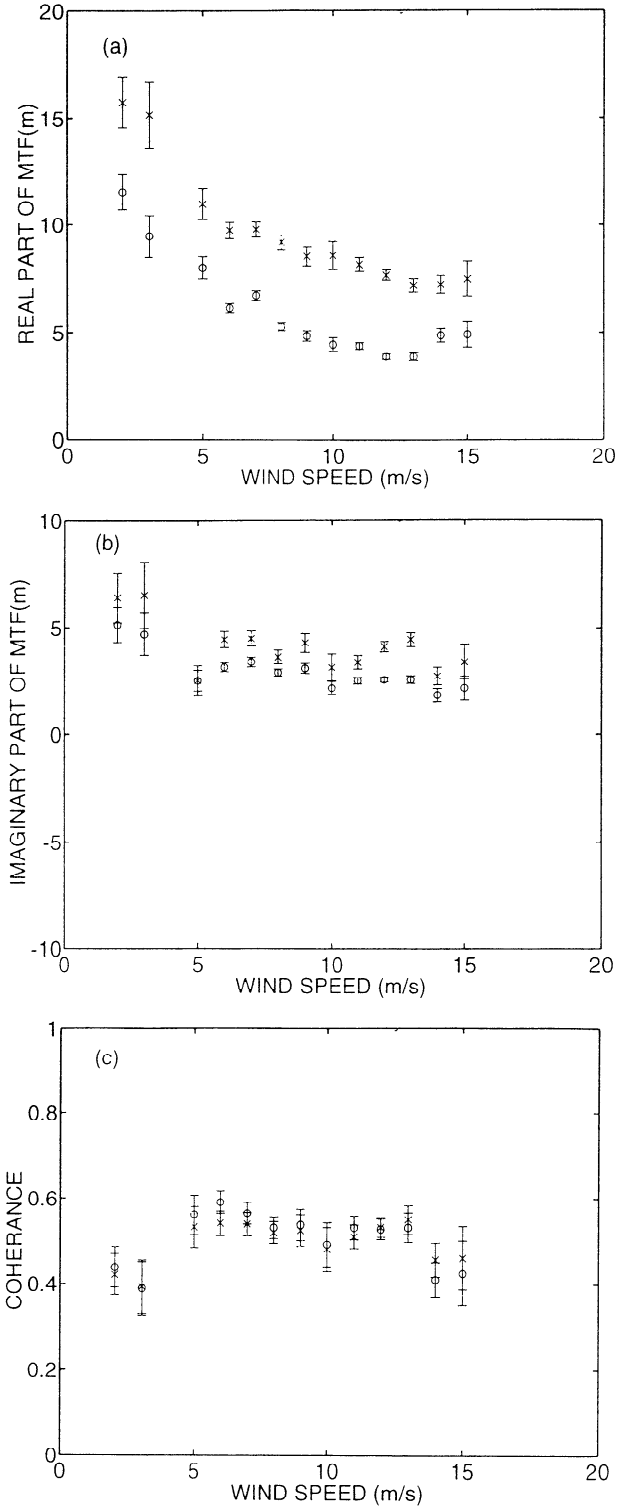

Figure 1. (a) Real and (b) imaginary parts of MTF(m) and (c) coherence(γ^2). SAXON-FPN experiment. Circles represent V polarization (pol), crosses represent H pol. Here $40° < \theta < 46°$; $|\phi_{wv}| < 30°$; $|\phi_{wd}| < 30°$; 0.25 Hz $< f <$ 0.3125 Hz. Error bars show 95% confidence level.

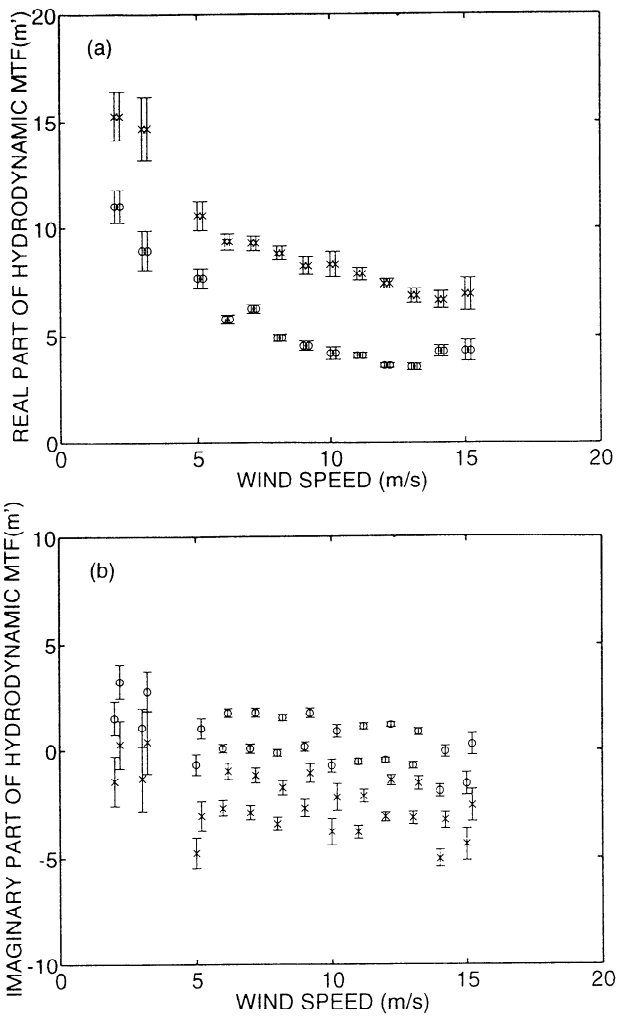

Figure 2. (a) Real and (b) imaginary parts of hydrodynamic MTF(m') with maximum and minimum tilt modulation. Results with maximum tilt modulation are slightly shifted to the right. Other conditions are same as Figure 1.

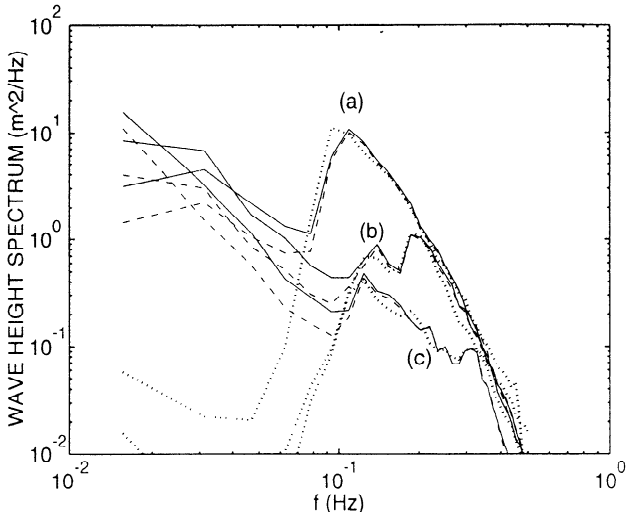

Figure 3. Wave height spectrum measured from H pol radar (solid line), V pol radar (dashed line), and buoy (dotted line). (a) Julian Day = 323–323.2, $\overline{U_{wd}}$ = 14.7 m s^{-1}, N_s = 23. (b) Julian Day = 324.8–325, $\overline{U_{wd}}$ = 9.8 m s^{-1}, N_s = 19. (c) Julian Day = 325.8–326, $\overline{U_{wd}}$ = 4.8 m s^{-1}, N_s = 23. $\overline{U_{wd}}$ is mean wind speed, and N_s is number of spectra averaged. SAXON-FPN experiment.

posite surface theory. We must therefore attempt to determine the cause of this failure of composite surface theory.

Let us first confirm that the FM part of the return indeed corresponds to the Doppler shift due to the long-wave orbital velocity. In Figure 3, long-wave frequency spectra calculated from the FM part of the return are plotted for both H pol and V pol. The conversion from the orbital velocity to the wave height has been done based on the linear wave theory and using the wave direction information from the buoy measurement. The spectrum calculated directly from the buoy data is also shown. Agreement among the three different measurements is rather good for the long-wave frequency range 0.1 Hz $< f <$ 0.35 Hz. (At higher frequencies the spectra are underestimated by microwave systems since the illuminated area becomes comparable to the wavelength of the long waves, while the spectra at lower frequencies are dominated by signal noise.) In particular, the results of H pol and V pol are almost identical in this range. This fact suggests that the microwaves are indeed scattered by surface features which are advected by the long-wave orbital velocity for both polarizations.

We next examine how the observed microwave cross sections compare with predictions of Bragg scattering theory for a slightly rough surface. According to the theory [e.g., *Plant*, 1990] the normalized cross section is written as (8) with the Bragg scattering geometric coefficient Γ given in (10) or (11). Therefore the ratio of σ_o of V pol to that of H pol is simply the ratio of the function Γ for V pol to Γ for H pol, which is 7.4 at $\theta = 46°$ and 4.7 at $\theta = 40°$. In Figure 4 the measured cross section for V pol is plotted versus that for H pol, where both measurements were performed simultaneously at

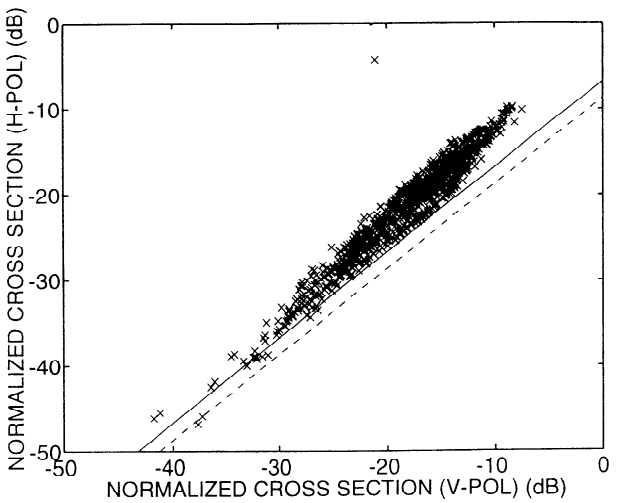

Figure 4. Normalized cross section σ_o of H pol versus that of V pol. The solid line is σ_{oV}/σ_{oH} = 4.7; the dashed line is σ_{oV}/σ_{oH} = 7.4. SAXON-FPN experiment. The 95% confidence interval is ±0.5 dB.

the same incidence angle θ between 40° and 46°. As detailed by *Plant et al.* [this issue (a)], 95% confidence intervals for these values are about ±0.5 dB when calibration and measurement uncertainties are combined. The two lines in Figure 4 correspond to the ratios of 4.7 and 7.4. When the cross section is small, that is, the wind speed is low, the measured ratio roughly follows the theoretical prediction. For higher wind speeds the H pol cross section is larger and/or the V pol cross section is smaller than the prediction based on the Bragg scattering theory by several decibels. This result is consistent with *Valenzuela* [1978], who has found that the V pol cross section agrees well with small perturbation theory, while the H pol cross section is several decibels larger in the same range of the incidence angle θ. This discrepancy has been found to increase further for larger θ. Although part of the discrepancy in H pol cross section can be attributed to the effect of finite mean square slope of long waves, Valenzuela has speculated that other scattering mechanisms must take place in H pol microwave scattering.

Recently *Kasilingam and Shemdin* [1992] and subsequently *Romeiser et al.* [this issue] have shown that the presence of intermediate-scale waves, which are much longer than Bragg resonant waves but shorter than the modulating long waves, can increase the "apparent" hydrodynamic MTF appreciably. A similar idea involving three-wavelength processes has also been proposed by *Thompson* [1988] for the modulation of X band radar backscatter by internal waves. The apparent hydrodynamic MTF in *Romeiser et al.* [this issue] corresponds to our definition of hydrodynamic MTF and is, perhaps, better termed the "residual" MTF. According to their calculation there are two major contributions from intermediate waves; one is due to the second-order tilt modulation and the other is the cross correlation between tilt and hydrodynamic modulations. Both of them are additional geometric effects associated with observation by a microwave system, and the "true" hydrodynamic MTF (i.e., the modulation of the wavenumber spectrum at the Bragg wavenumber) is hardly affected by intermediate-scale waves. They also show that these effects are much stronger for H pol because of the larger value of tilt modulations. Their model is consistent with our observations and suggests that our calculation of hydrodynamic MTF overestimates the true hydrodynamic MTF, in particular for H pol. Instead of subtracting the effect of intermediate-scale waves from our observed total MTF, a procedure which requires more unknown parameters such as the wavenumber spectrum and the MTF of the intermediate-scale waves, we choose to use our estimate of hydrodynamic MTF for V pol in the following discussion to attempt to infer modulated wind stress from the measurements. We emphasize that our V pol values may serve only as the upper limit of the true hydrodynamic MTF and therefore that we may be slightly overestimating the modulation of the wind stress also. Despite this uncertainty as to the measured value of the true hydrodynamic MTF, we believe the following discussion is a useful analysis to understand the physical mechanism of the hydrodynamic modulation of very short gravity-capillary waves by long waves.

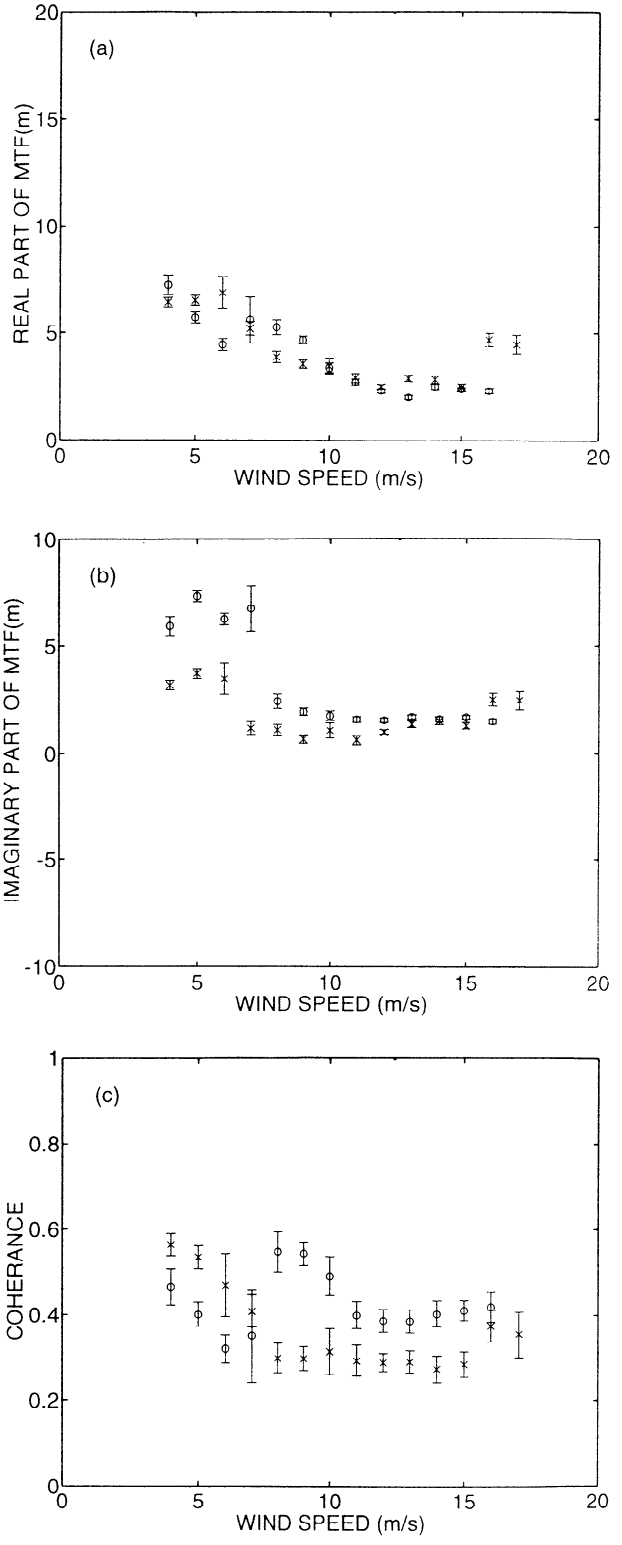

Figure 5. (a) Real and (b) imaginary parts of MTF(m) and (c) coherence(γ^2). MARSEN experiment. V pol. Circles represent $40° < \theta < 45°$, crosses represent $55° < \theta < 60°$. Here $|\phi_{wv}| < 30°$; $|\phi_{wd}| < 30°$; 0.25 Hz $< f <$ 0.3125 Hz. Error bars show 95% confidence level.

3.3. Comparison for Different Incidence Angles

In the MARSEN experiment most of the data were V pol, but the incidence angle θ varied between 40° and 70°. Since the return power strongly depends on θ, the magnitude of the tilt modulation m_t varies with θ. Although the resonant Bragg wavenumber $k = 2k_o \sin\theta$ is also modified with θ, the slope of the folded wavenumber spectrum ψ is not likely to change significantly with the slight change of the Bragg wavenumber k. Therefore the hydrodynamic MTF should be roughly independent of the incidence angle θ. We show the total and the hydrodynamic MTF in Figure 5 and Figure 6 for V pol and for different θs. As expected, the real parts of both MTFs do not show any explicit dependence on θ, while the imaginary part of the total MTF is larger for smaller θ when the wind is weak. As the wind speed increases, this difference decreases. When the tilt modulation is subtracted, the difference between small and large θs almost disappears in the intermediate wind speed range (8–11 $\mathrm{m\,s^{-1}}$), which is consistent with the theoretical predictions. For weaker wind the subtraction of m_t is not sufficient to eliminate the difference; there are two possible explanations for this. It has been reported that the wavenumber spectrum has a larger slope around k = 1–2 $\mathrm{cm^{-1}}$ when the wind is weak [*Jähne and Riemer*, 1990]. A similar dip was also observed by *Wright and Keller* [1971] around k = 1–3 $\mathrm{cm^{-1}}$. Since the Bragg resonant wavenumber for this experiment was k = 2.7–3.6 $\mathrm{cm^{-1}}$, it was possible that the actual slope of the spectrum was much larger than that in (26), and that the slope of the spectrum was larger for smaller k (i.e., smaller θ). Both possibilities tend to decrease the observed difference of the imaginary part of m' between large and small incidence angles. For strong wind the subtraction of the tilt modulation slightly overcompensates the difference of the imaginary part of m'. This may indicate either that the folded wavenumber spectrum has gentler slope or that the return signal depends on scattering mechanisms other than Bragg resonance. It is also possible that the basic linear assumption is violated for such strong winds.

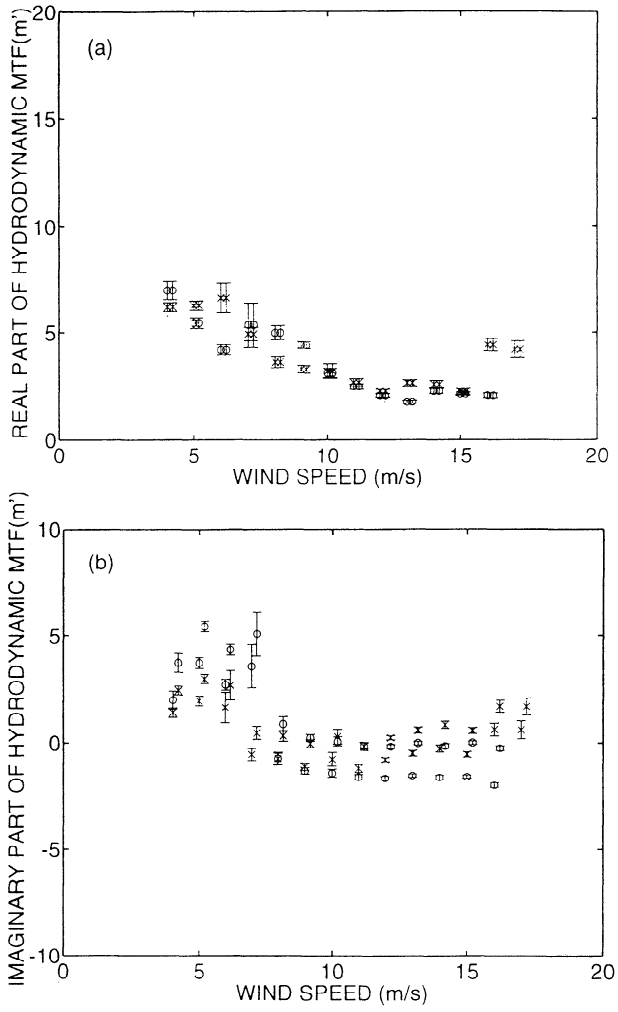

Figure 6. (a) Real and (b) imaginary parts of hydrodynamic MTF(m') with maximum and minimum tilt modulation. Results with maximum tilt modulation are slightly shifted to the right. Other conditions are same as Figure 5.

3.4. Comparison Between Different Experiments

To compare the results of MARSEN and SAXON-FPN, we show the magnitude and phase of the hydrodynamic MTF for V pol from both experiments in Figure 7. Agreement is reasonable except that the MARSEN data show a lower MTF for strong winds. The phase of m' slightly decreases with wind speed but is always near zero, indicating that the wavenumber spectrum maximizes near the long-wave crest.

Recently, *Miller and Shemdin* [1991] measured the hydrodynamic modulation of slope frequency spectra between 13–26 Hz with mechanically generated waves of 0.5 Hz. Although the long-wave frequency is different, the observed phase of the frequency MTF (50° at U_{wd} = 4 $\mathrm{m\,s^{-1}}$ decreasing to 0° at U_{wd} = 10 $\mathrm{m\,s^{-1}}$) is roughly consistent with ours. The magnitude of the frequency MTF first decreases with wind speed (4–5 at U_{wd} = 4 $\mathrm{m\,s^{-1}}$ to 3–4 at U_{wd} = 6.4 $\mathrm{m\,s^{-1}}$) and then increases (5–7 at U_{wd} = 9–10 $\mathrm{m\,s^{-1}}$). They speculate that their frequency MTF is about one half of the conventional hydrodynamic MTF, since the frequency spectra include waves propagating in all directions, and those propagating away from the long-wave direction are modulated less by the long-wave orbital velocity. Then their results at U_{wd} = 4–6.4 $\mathrm{m\,s^{-1}}$ are consistent with our observations, while those at U_{wd} = 9–10 $\mathrm{m\,s^{-1}}$ are much larger than ours. However, as the relaxation rate increases relative to the long-wave frequency, the short-wave modulation becomes more uniform in all propagation directions, as will be shown in section 4.2. Therefore, by our definition, for strong winds the frequency MTF should be closer to the hydrodynamic MTF. Miller and Shemdin's observations then may be consistent with ours even at higher winds.

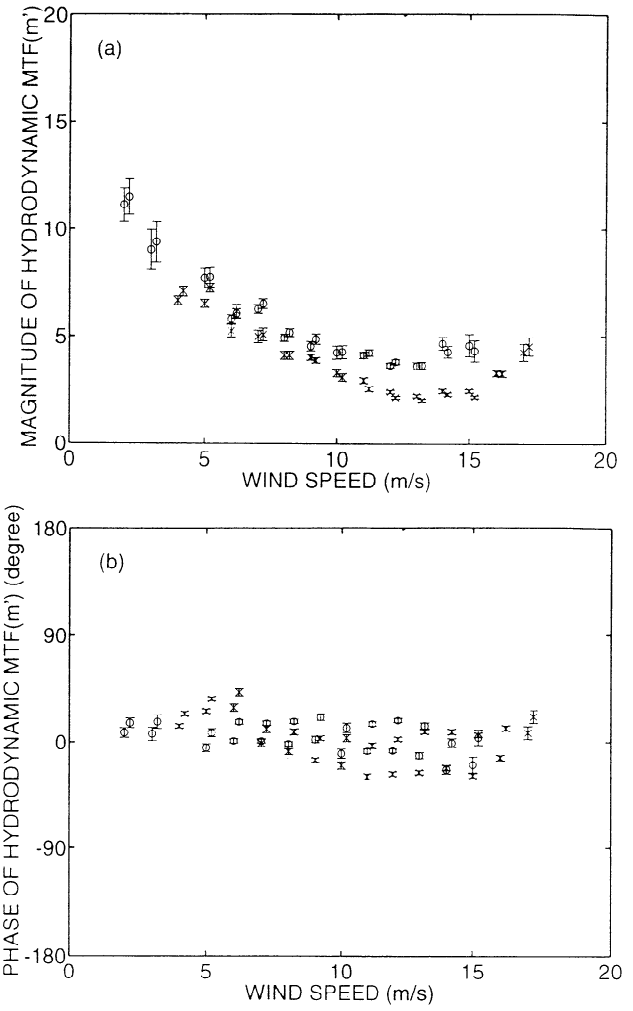

Figure 7. (a) Magnitude and (b) phase of hydrodynamic MTF(m') with maximum and minimum tilt modulation. Results with maximum tilt modulation are slightly shifted to the right. V pol. Circles represent SAXON-FPN experiment, $40° < \theta < 46°$; crosses represent MARSEN experiment, $40° < \theta < 60°$. Here $|\phi_{wv}| < 30°$; $|\phi_{wd}| < 30°$; 0.25 Hz $< f <$ 0.3125 Hz. Error bars show 95% confidence level.

4. Estimates of Shear Stress Modulation Along the Long-Wave Profile

4.1. Normally Incident Waves and Wind

In section 2 we derived the hydrodynamic MTF from the relaxation model. Since we now have an experimental estimate of m', it is in turn possible to estimate the wind shear stress modulation along the long-wave profile. Note that since we have not subtracted the effect of intermediate-scale waves, our values of m' tend to be the upper limit of the true hydrodynamic MTF.

Let us calculate m_{∞} defined in (39) from (38) and measured values of m'. Inside the square brackets of (38) the derivatives of $\bar{F}$ are first replaced by those of $\bar{\psi}$ and evaluated using (25). The phase velocity c and the group velocity c_g of the Bragg resonant waves are calculated based on the linear theory. The relaxation rate β is first assumed to be equal to the wind growth rate

$$\beta_{wd} = 0.04\omega \left(\frac{u_*}{c}\right)^2 |\cos\phi_{wd}| \tag{57}$$

after *Plant* [1982]. This corresponds to the assumption that the nonlinear term in the total forcing in the action conservation equation is quadratic (see (47)). The friction velocity u_* is empirically related to the wind speed U_{wd} based on the direct measurement of u_* by Siegfried Stolte during part of the SAXON-FPN experiment. The results are shown in Figure 8. Recall that m_{∞} is related to the wind shear stress modulation along the long waves by (40). According to *Jähne and Riemer* [1990] the equilibrium wavenumber spectrum F_{eq} is proportional to $u_*^{2.5}$ for the wavenumbers corresponding to X band. Therefore m_{∞} is roughly 2.5 times the friction

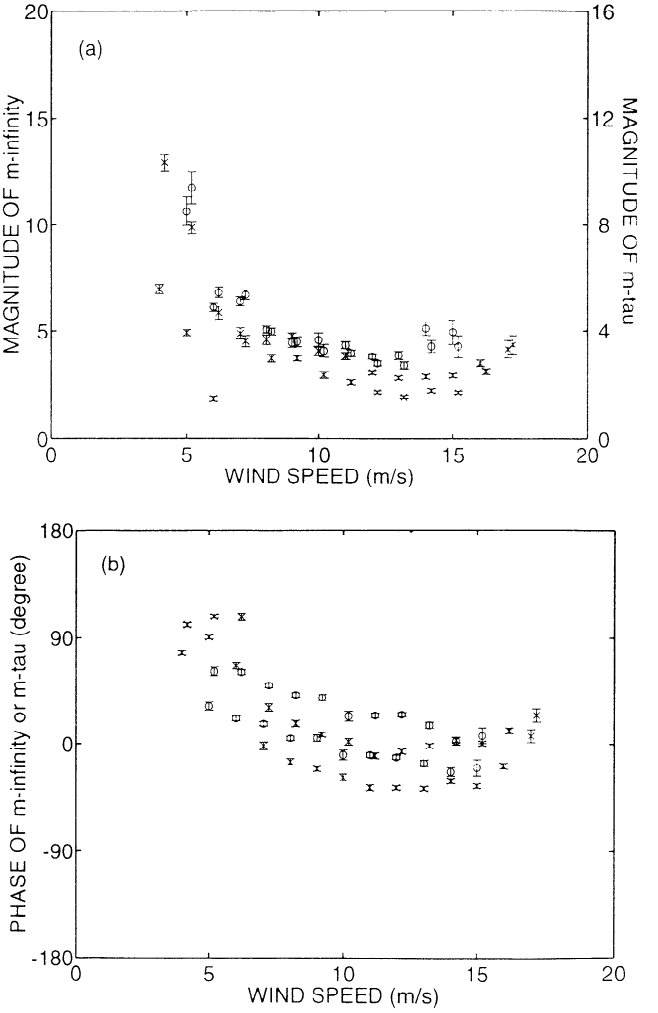

Figure 8. (a) Magnitude and (b) phase of m_{∞} and m_{τ} with maximum and minimum tilt modulation. Results with maximum tilt modulation are slightly shifted to the right. V pol. Circles represent SAXON-FPN experiment, $40° < \theta < 46°$; crosses represent MARSEN experiment, $40° < \theta < 60°$. Here $|\phi_{wv}| < 30°$; $|\phi_{wd}| < 30°$; 0.25 Hz $< f <$ 0.3125 Hz. Error bars show 95% confidence level. Relaxation rate is equal to the wind growth rate.

velocity modulation $\frac{C}{\bar{u}_*}\frac{G_{u_*U}}{G_{UU}}$, or 1.25 times the shear stress modulation $\frac{C}{\bar{\tau}}\frac{G_{\tau U}}{G_{UU}}$, where $\tau = \rho u_*^2$ and ρ is the density of air. We denote the shear stress modulation by m_τ, and its values are also shown on the right-hand side of Figure 8.

For wind speeds larger than $10\,\mathrm{m\,s^{-1}}$, m_∞ is almost identical to m' shown in Figure 7, indicating that the relaxation is much faster than the long-wave frequency. This means that the modulation of the short-wave spectrum is determined solely by the wind shear stress modulation along the long waves. As the wind speed decreases, the effect of straining due to the long-wave orbital velocity becomes important. The magnitude of m_∞ remains close to that of m', whereas the phase of the m_∞ gradually increases compared with that of m', indicating that the shear stress maximum occurs slightly ahead of the long-wave crest. For wind speeds less than $5\,\mathrm{m\,s^{-1}}$, the magnitude of m_∞ increases rapidly. However, the growth rate β in this range is so small that the accuracy of the m_∞ calculated from (38) is questionable. We also show the results assuming that the relaxation rate β is twice the wind growth rate β_{wd} (i.e., the nonlinear term in the forcing term of the action conservation equation is cubic, see (47)) in Figure 9. Since the relaxation rate is larger, m_∞ and m' are closer at low wind speeds. At intermediate to high wind speeds the effect of increasing β is small.

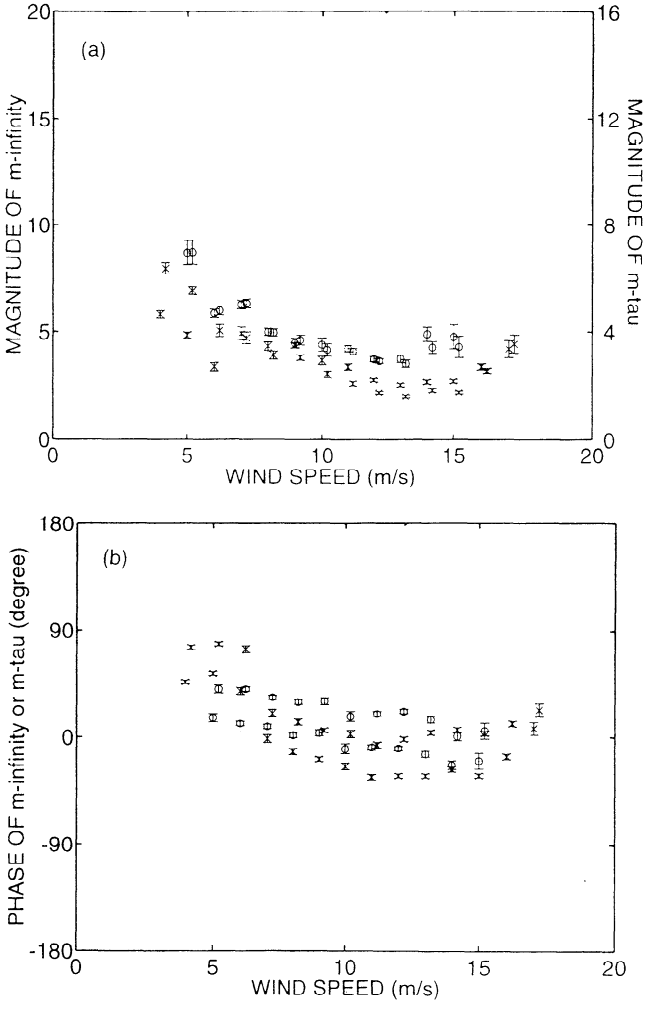

Figure 9. Same as Figure 8 except relaxation rate is twice the wind growth rate.

In Figure 7 of *Wright et al.* [1980] they show the modulated source function S_u, which corresponds to βm_∞ by our definition. Using the values of $\beta = \beta_{wd}$, given in (57) of this paper, their results for the long-wave frequency 0.30 Hz yield $m_\infty = 11.3$, 5.2, and 3.0 for wind speeds $U_{wd} = 6$, 8, and $10\,\mathrm{m\,s^{-1}}$, respectively. Except for the weakest wind the results are consistent with ours.

So far measurements of the modulated wind shear stress have not been conducted on the scale of dominant ocean surface waves. On a laboratory scale *Hsu et al.* [1981] and *Hsu and Hsu* [1983] have measured the modulation of the turbulent momentum flux by mechanically generated waves of 1 Hz with wind speed $U_{wd} = 1.37$–$2.92\,\mathrm{m\,s^{-1}}$. Although the long-wave length and the wind speed are much smaller than those of the present study, it is worth noting that the laboratory results for the phase of m_τ is always close to 90°, being somewhat consistent with our results for very weak wind. The magnitude of m_τ in laboratory experiments is estimated to be 4–6 if averaged over 0–5 cm from the water surface, although m_τ decreases with height rather quickly. Again, the order of magnitude seems to be consistent with our deduced values.

We have also examined the results of the L band V pol system from the MARSEN experiment. It has been found that the calculated hydrodynamic MTF is independent of the wind speed; its magnitude is around 4-5, and its phase is close to zero. Since the Bragg wavenumber of the L band system is roughly 1/8 and the relaxation rate is only 1/20 as large as those of the X band system, the effect of modulated wind stress is generally small relative to the modulation by long-wave orbital velocity according to our relaxation model: The observation is consistent with the prediction by the hydrodynamic model. It is desirable to obtain more data at intermediate Bragg wavenumbers in order to confirm our hydrodynamic model.

4.2. Obliquely Incident Waves and Wind

We next examine the case of wind and waves propagating obliquely to the antenna look direction from the SAXON-FPN data. As mentioned earlier, we ascertained that the wind and wave directions are close when the long-wave frequency is 0.25 Hz or higher. In the following figures the wind angle is restricted to within ±30° of the wave direction. For very weak winds the hydrodynamic MTF m' is dominated by straining due to the long-wave orbital velocity (square bracket in (38)), which decreases to zero as the wave angle increases. As the wind speed increases m' approaches m_∞. Since the shear stress modulation along the long-wave profile is independent of the antenna look direction, the phase of m_∞ must be independent of the wave angle. Furthermore, the dependence of the equilibrium wavenumber spectrum F_{eq} on the friction velocity u_* is roughly in-

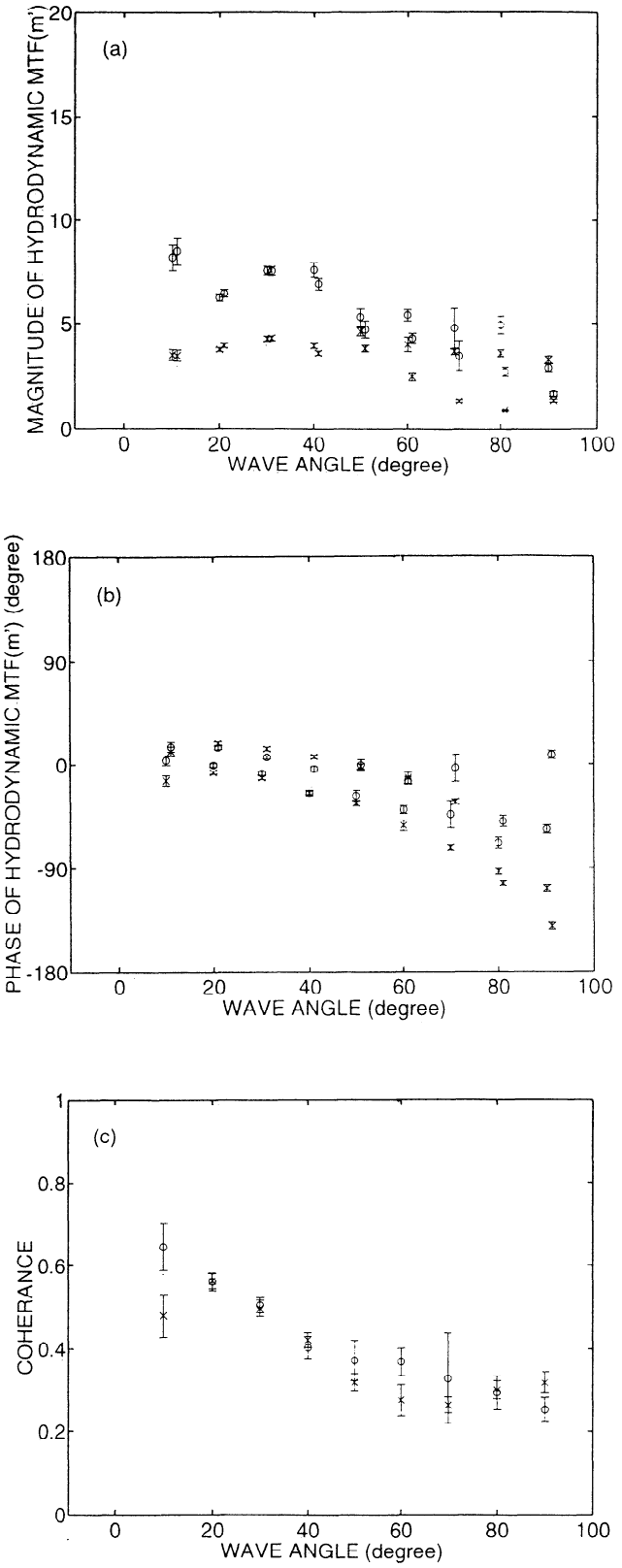

Figure 10. (a) Magnitude and (b) phase of hydrodynamic MTF(m') with maximum and minimum tilt modulation, and (c) coherence. Results with maximum tilt modulation are slightly shifted to the right. SAXON-FPN experiment. V pol. Circles represent $U_{wd} = 6 \pm 1\,\mathrm{m\,s^{-1}}$; crosses represent $U_{wd} = 12 \pm 1\,\mathrm{m\,s^{-1}}$. Here $|\phi_{wd} - \phi_{wv}| < 30°$; 0.25 Hz $< f <$ 0.3125 Hz. Error bars show 95% confidence level.

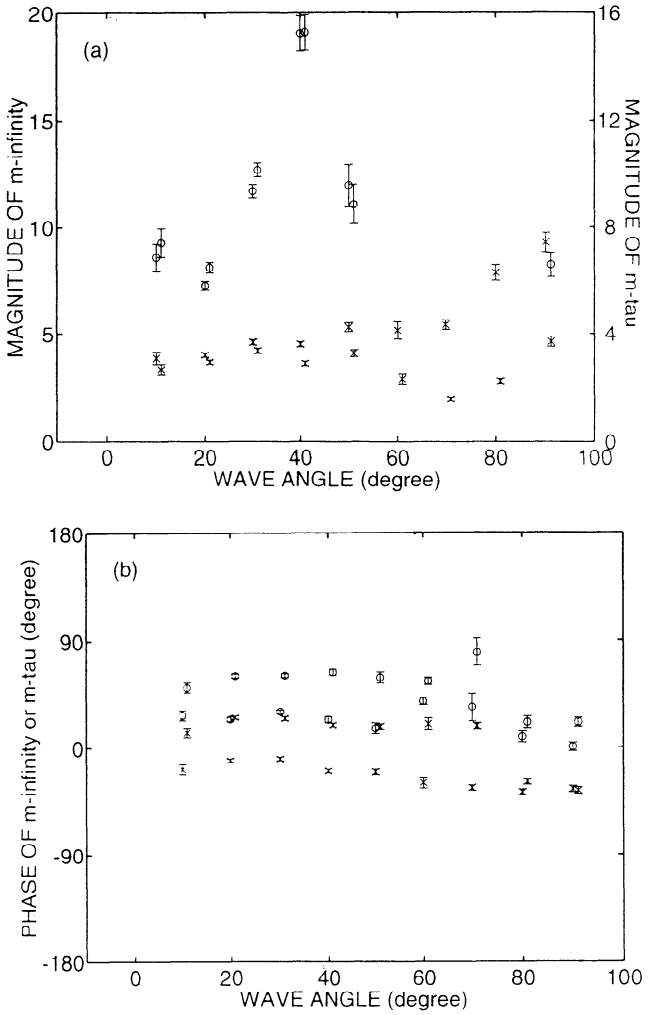

Figure 11. (a) Magnitude and (b) phase of m_∞ and m_τ. Relaxation rate is equal to the wind growth rate. Other conditions are same as Figure 10.

dependent of the wind direction [*Jähne and Riemer*, 1990]. Therefore the magnitude of m_∞ should also be roughly independent of the wave angle.

We first show the hydrodynamic MTF(m') for different wave angles and for two wind speeds in Figure 10. For both wind speeds the phase of m' decreases as the wave angle increases. The magnitude of m' decreases monotonically at $U_{wd} = 6\,\mathrm{m\,s^{-1}}$, while it remains almost constant up to $\phi_{wv} = 60°$ at $U_{wd} = 12\,\mathrm{m\,s^{-1}}$, suggesting the increased effect of the wind shear modulation. Although the coherence decreases as the wind/wave angle increases, it remains around 0.3, indicating that a significant part of the modulation of the Bragg wave spectrum is still correlated with long waves.

Next the estimate of m_∞ or m_τ with the assumption $\beta = \beta_{wd}$, given in (57), is shown in Figure 11. The phase of m_∞ is fairly constant as predicted, and the magnitude of m_∞ for $U_{wd} = 12\,\mathrm{m\,s^{-1}}$ is stable up to $\phi_{wv} = 70°$, while the magnitude for $U_{wd} = 6\,\mathrm{m\,s^{-1}}$ becomes unbounded for large wave angle because of the small relaxation rate. For waves propagating off

the wind direction the relaxation rate is not necessarily determined by the wind growth rate only. In the extreme case, nonlinear wave interactions transfer energy so quickly among waves of different directions that the modulation of the spectrum occurs uniformly in all directions. In this case the relaxation rate is independent of the propagation direction. We therefore calculate the m_∞ (or m_τ) assuming that the relaxation rate is identical to the wind growth rate of normally incident waves, that is, $\beta = \beta_{wd}$ ($\phi_{wd} = 0$). The results are shown in Figure 12. In this case the magnitude of m_∞ remains fairly constant for both wind speeds. The phase of m_∞ for $U_{wd} = 12\,\mathrm{m\,s^{-1}}$ also remains steady, although the phase for $U_{wd} = 6\,\mathrm{m\,s^{-1}}$ decreases with ϕ_{wv}. In reality the relaxation rate is probably somewhere between the two extreme cases examined.

5. Hydrodynamic MTFs From the Gulf of Mexico

We next examine the data from the Gulf of Mexico experiment which took place in November and December, 1978 (see *Keller et al.* [1985] for details). The experiment was performed with a V pol X band microwave system at an incidence angle $\theta = 45°$. The duration of the experiment was divided into two very different regimes. When a cold front passed, the wind

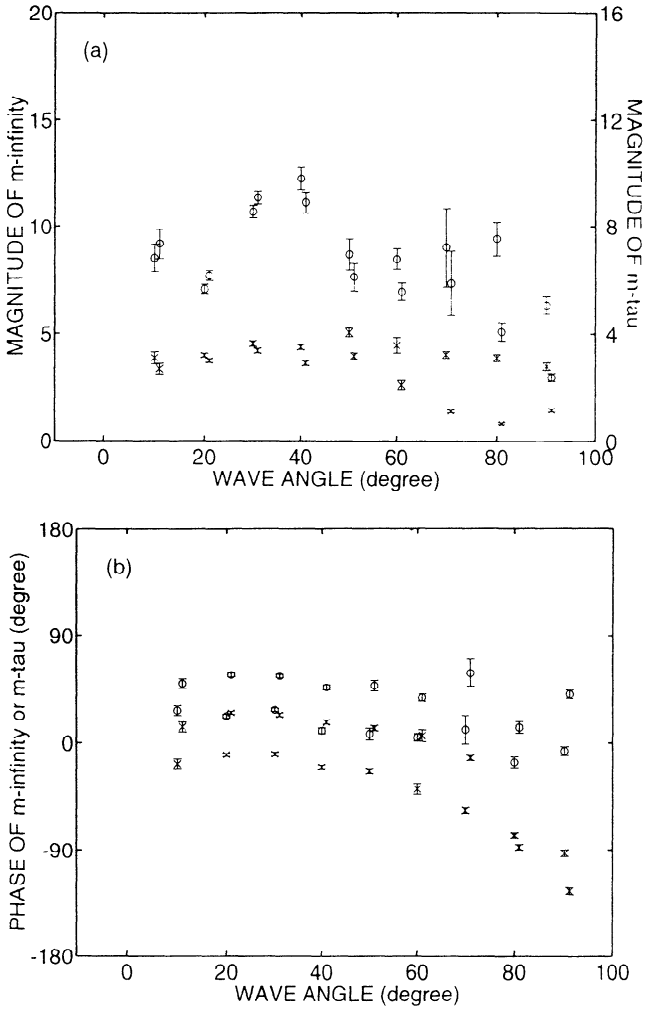

Figure 12. (a) Magnitude and (b) phase of m_∞ and m_τ. Relaxation rate is equal to the wind growth rate at $\phi_{wd} = 0$. Other conditions are same as Figure 10.

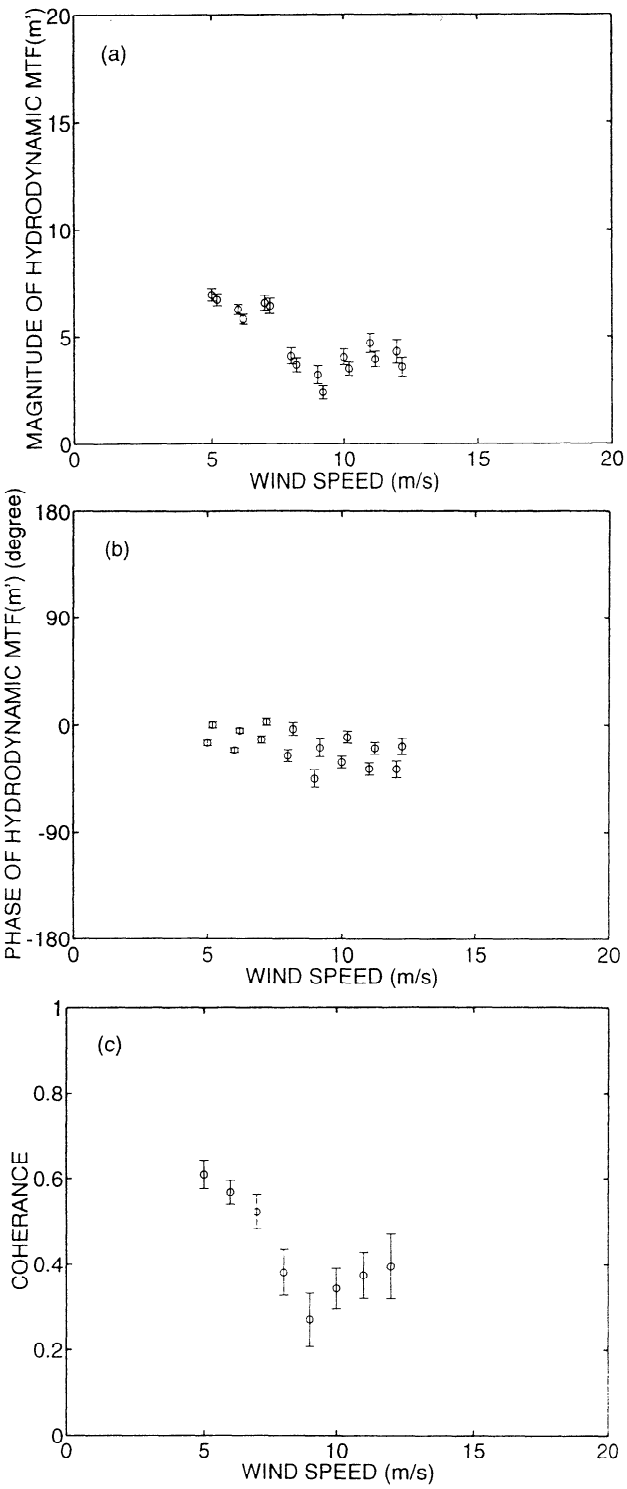

Figure 13. (a) Magnitude and (b) phase of hydrodynamic MTF(m') with maximum and minimum tilt modulation, and (c) coherence. Results with maximum tilt modulation are slightly shifted to the right. Gulf of Mexico experiment. V pol. Here $|\phi_{wv}| < 30°$; $|\phi_{wd}| < 30°$; 0.25 Hz $< f <$ 0.3125 Hz; $-18°\mathrm{C} < \Delta T < -6°\mathrm{C}$. Error bars show 95% confidence level.

was mostly from the north and the air temperature relative to the water temperature, denoted by ΔT, was between $-18°C$ and $-6°C$. At other times the wind was from between south and east, and ΔT was always larger than $-6°C$. We first present the hydrodynamic MTF and the coherence from the first regime in Figure 13. Both the magnitude and the phase are consistent with the results from SAXON-FPN and MARSEN, although the atmospheric stability is quite different. It seems that the atmospheric stability does not affect the hydrodynamic MTF appreciably under unstable conditions. We have also ascertained that m' is independent of the mean square long-wave slope denoted by s (see also *Keller et al.* [1985]). Next, the hydrodynamic MTF and the coherence from the second regime are presented in Figure 14. We first note that the hydrodynamic MTF from the second regime is much larger and scatters significantly. It has also been observed that m' strongly depends on the mean square long-wave slope s as is shown in Figure 14. When the long-wave slope is relatively large, the results are rather close to those in the first regime or in other experiments. As the long-wave slope decreases, the magnitude of m' increases rapidly. This deviation seems to disappear for the wind speed $U_{wd} > 11\,\mathrm{m\,s^{-1}}$ but becomes significant for weaker winds.

From these observations we suspect the presence of a unique environmental condition with the following characteristics: (1) observed in the Gulf of Mexico but not in the North Sea, (2) Observed only when the air-sea interface is neutrally stable, (3) Observed only when the sea state is low (i.e., mean square long-wave slope is small), (4) Observed when the wind speed is lower than $11\,\mathrm{m\,s^{-1}}$. One strong candidate is the presence of surface contamination. It is well known that surface films suppress the short-wave spectrum in the gravity-capillary range. Since surface films cannot survive when the surface mixing is strong, items (2) to (4) are qualitatively consistent. Furthermore, the laboratory observations by Feindt (reported in *Alpers and Hühnerfuss* [1989]) have shown that the effect of surface films on the short-wave spectrum disappears when the wind speed exceeds $12\,\mathrm{m\,s^{-1}}$. Since the wavenumber spectrum drops more rapidly with decreasing wind speed when the film is present (see Figure 5 of *Alpers and Hühnerfuss* [1989]), the magnitude of m_∞ is expected to increase with films (see (40)). Physically, near the trough where the wind stress is relatively small, the enhanced dissipation by surface films is more effective in reducing the Bragg wave spectrum, while the film effect is overshadowed by a stronger wind input near the crest. This effectively emphasizes the contrast between short-wave spectra at crests and at troughs, thus increasing the hydrodynamic MTF. Surface films may also influence the relaxation rate, the shape of the wavenumber spectrum, and the wind shear modulation along the long waves. In particular, it has been observed that films strongly dampen a certain range of wavenumbers, resulting in a 'dip' in the short-wave spectrum. Depending on the location of this dip relative to the Bragg wavenumber, the slope of the spectrum $\frac{k}{F}\frac{\partial F}{\partial k}$ can be either increased or decreased. For a more quantitative analysis of the effect of films on the hydrodynamic MTF, it is necessary to investigate independently how the film may affect the relaxation rate β, the wavenumber spectrum, and the shear stress modulation along

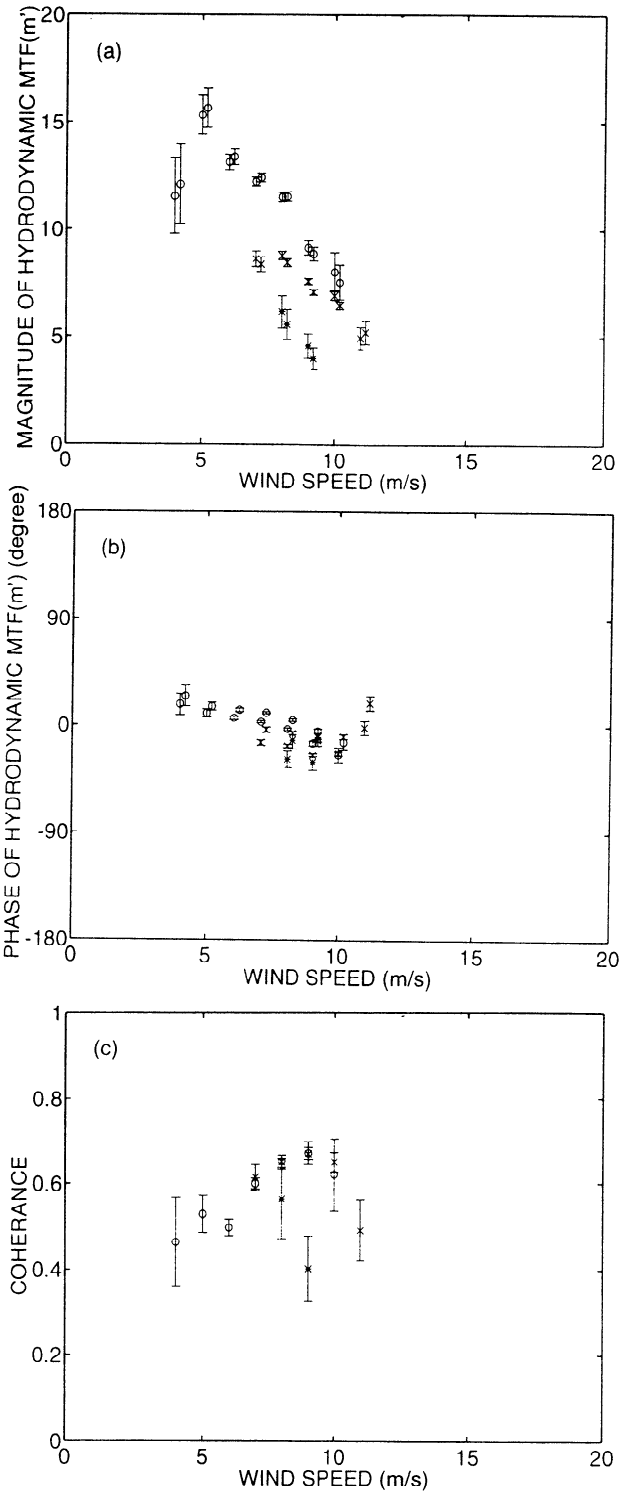

Figure 14. (a) Magnitude and (b) phase of hydrodynamic MTF(m') with maximum and minimum tilt modulation, and (c) coherence. Circles represent $0 < s < 0.002$; crosses represent $0.002 < s < 0.004$; asterisks represent $0.004 < s$. Here $-6°C < \Delta T < 3°C$. Other conditions are same as Figure 13.

long waves. These will be the subjects of future investigations.

6. Concluding Remarks

A simplified relaxation model for the hydrodynamic modulation of gravity-capillary wave spectra by long waves has been proposed. The model is based on the relaxation rate and the equilibrium short-wave wavenumber spectrum as a function of local wind stress; detailed knowledge of the forcing terms, such as wind input, nonlinear wave-wave interaction, or nonlinear dissipation, is not required. For longer gravity-capillary wavelengths corresponding to L band, the model indicates that the hydrodynamic MTF is primarily due to straining by long-wave orbital velocities except perhaps at very high wind speeds. This prediction of the model seems to be supported by the MARSEN L band results. On the other hand, for short wavelengths corresponding to the Bragg wavelength for X band, the model indicates that at moderate to strong wind speeds the hydrodynamic MTF is mostly due to the wind shear stress modulation and that the effect of straining by long-wave orbital velocity is weak. The model has been employed in combination with X band microwave backscatter measurements to estimate the wind shear stress distribution along the long-wave profile. The results are qualitatively consistent with past laboratory studies, although quantitative confirmation of our hydrodynamic model will not be possible until reliable measurements of modulated wind stress in a field environment are performed. The results at different wind-wave angles suggest that the relaxation rate of short wind waves propagating off the wind direction is larger than that estimated from the wind energy input rate alone.

We have calculated the hydrodynamic MTF at X band from past experimental data and compared the results for different polarizations, incidence angles, and locations. The magnitude of the hydrodynamic MTF from H pol microwave systems has been found to be larger than that from V pol, the difference being on the order of four. This result indicates a problem with the traditional composite surface-scattering theory as it has been applied to MTF calculations. *Romeiser et al.* [this issue] point out that geometric effects related to intermediate-scale waves have been previously neglected in MTF calculations based on composite surface theory. Upon including these intermediate scales, they find an increase of the apparent hydrodynamic MTF for H pol return, in qualitative agreement with the present results.

Measurements at different incidence angles yield consistent results for the hydrodynamic MTF for intermediate wind speeds, while the data scatter significantly for very weak winds. The agreement between SAXON-FPN and MARSEN experiments is reasonable except for strong winds. While the hydrodynamic MTFs from the Gulf of Mexico experiment agree with MARSEN and SAXON-FPN measurements for unstable conditions, near neutral stability they are much larger than those in other locations. We suspect that the existence of surface films may be the source of this deviation.

In order to further our understanding of the modulation of short wind waves due to long waves, it is necessary to study independently how the wind shear stress is modulated by long waves and how the wavenumber spectrum adjusts itself to a new equilibrium state (relaxation rate). According to *Gent and Taylor* [1976] the shear stress profile along long waves is sensitive to the surface roughness distribution. Since gravity-capillary waves are a major source of surface roughness, the modulation of gravity-capillary waves and the modulation of wind shear stress are probably coupled together, rather than one being determined by the other. Both experimental and theoretical studies are needed to understand this complicated physical process.

Finally, more studies are needed to understand the effect of surface contamination on short wind wave dynamics since this seems to play an important role when wind is weak.

Acknowledgments. This research was supported by ONR grant N00014-89-J-1897. This is WHOI contribution 8034.

References

Alpers, W., and K. Hasselmann, The two-frequency microwave technique for measuring ocean-wave spectra from an airplane or satellite, *Boundary Layer Meteorol., 13*, 215-230, 1978.

Alpers, W., and H. Hühnerfuss, The damping of ocean waves by surface films: A new look at an old problem, *J. Geophys. Res., 94*, 6251-6265, 1989.

Alpers, W., D.B. Ross, and C.L. Rufenach, On the detectability of ocean surface waves by real and synthetic aperture radar, *J. Geophys. Res., 86*, 6481-6498, 1981.

Bendat, J.S., and A.G. Piersol, *Random Data*, Wiley-Interscience, New York, 1986.

Gent, P.R., and P.A. Taylor, A numerical model of the air flow above water waves, *J. Fluid Mech., 77*, 105-128, 1976.

Hsu, C.T., and E.Y. Hsu, On the structure of turbulent flow over a progressive water wave: Theory and experiment in a transformed, wave-following coordinate system, 2, *J. Fluid Mech., 131*, 123-153, 1983.

Hsu, C.T., E.Y. Hsu, and R.L. Street, On the structure of turbulent flow over a progressive water wave: Theory and experiment in a transformed, wave-following co-ordinate system, *J. Fluid Mech., 105*, 87-117, 1981.

Jähne, B., and K.S. Riemer, Two-dimensional wave number spectra of small-scale water surface waves, *J. Geophys. Res., 95*, 11,531-11,546, 1990.

Kasilingam, D.H., and O.H. Shemdin, The validity of the composite surface model and its applications to the modulation of radar backscatter, *Int. J. Remote Sens., 13*, 2079-2104, 1992.

Keller, W.C., and W.J. Plant, Cross sections and modulation transfer functions at L and Ku bands measured during the Tower Ocean Wave and Radar Dependence Experiment, *J. Geophys. Res., 95*, 16,277-16,289, 1990.

Keller, W.C., and J.W. Wright, Microwave scattering and the straining of wind-generated waves, *Radio Sci, 10*, 139-147, 1975.

Keller, W.C., W.J. Plant, and D.E. Weissman, The dependence of X band microwave sea return on atmospheric

stability and sea state, *J. Geophys. Res., 90*, 1019-1029, 1985.

Larson, T.R., and J.W. Wright, Wind-generated gravity-capillary waves: Laboratory measurements of temporal growth rates using microwave backscatter, *J. Fluid Mech., 70*, 417-436, 1975.

Miller, S.J., and O.H. Shemdin, Measurement of the hydrodynamic modulation of centimeter-waves, *J. Geophys. Res., 96*, 2749-2759, 1991.

Phillips, O.M., Spectral and statistical properties of the equilibrium range in wind-generated gravity waves, *J. Fluid Mech., 156*, 505-531, 1985.

Plant, W.J., A relationship between wind stress and wave slope, *J. Geophys. Res., 87*, 1961-1967, 1982.

Plant, W.J., The modulation transfer function: Concept and applications, in *Radar Scattering From Modulated Wind Waves*, edited by G.J. Komen and W.A. Oost, pp. 155-172, Kluwer Academic Publishers, Dordrecht, Netherlands, 1989.

Plant, W.J., Bragg scattering of electromagnetic waves from the air/sea interface, in *Surface Waves and Fluxes, vol. 2*, edited by G.L. Geernaert and W.J. Plant, pp. 41-108, Kluwer Academic Publishers, Dordrecht, Netherlands, 1990.

Plant, W.J., and W. Alpers, An introduction to SAXON-FPN, *J. Geophys. Res.*, this issue.

Plant, W.J., W.C. Keller, and A. Cross, Parametric dependence of ocean wave-radar modulation transfer functions, *J. Geophys. Res., 88*, 9747-9756, 1983.

Plant, W.J., E.A. Terray, R.A. Petitt, and W.C. Keller, The dependence of microwave backscatter from the sea on illuminated area: Correlation times and lengths, *J. Geophys. Res.*, this issue (a).

Plant, W.J., W.C. Keller, E.A. Terray, and R.A. Petitt, Microwave backscatter from the sea: The modulation of received power and Doppler bandwidth by long waves, *J. Geophys. Res.*, this issue (b).

Romeiser, R., A. Schmidt, and W. Alpers, A three-scale composite surface model for the ocean wave-radar modulation transfer function, *J. Geophys. Res.*, this issue.

Schröter, J., F. Feindt, W. Alpers, and W.C. Keller, Measurement of the ocean wave-radar modulation transfer function at 4.3 GHz, *J. Geophys. Res., 91*, 923-932, 1986.

Smith, J.A., Modulation of short wind waves by long waves, in *Surface Waves and Fluxes, vol. 1*, edited by G.L. Geernaert and W.J. Plant, pp. 247-284, Kluwer Academic Publishers, Dordrecht, Netherlands, 1990.

Thompson, D.R., Calculation of radar backscatter modulations from internal waves, *J. Geophys. Res., 93*, 12,371-12,380, 1988.

Valenzuela, G.R., Theories for the interaction of electromagnetic and oceanic waves: A review, *Boundary Layer Meteorol., 13*, 61-85, 1978.

Wright, J.W., and W.C. Keller, Doppler spectra in microwave scattering from wind waves, *Phys. Fluids., 14*, 466-474, 1971.

Wright, J.W., W.J. Plant, and W.C. Keller, Ocean wave-radar modulation transfer functions from the West Coast Experiment, *J. Geophys. Res., 85*, 4957-4966, 1980.

T. Hara, Graduate School of Oceanography, University of Rhode Island, Narragansett, RI 02882.

W. J. Plant, Applied Physics Laboratory, University of Washington, Seattle, WA 98105.

(Received June 16, 1993; revised December 13, 1993; accepted December 13, 1993.)